Hydrodynamic Techniques for Study of Wind Effects on Antenna Structures

By K. N. COYNE

(Manuscript received June 1, 1965)

The effects of random wind-induced torques and structural loading are described and evaluated in terms of antenna performance, pointing errors, and overturning stability. A model test theory is developed to utilize economical small scale models to accurately determine drag torque coefficients of complex asymmetrical structures, using water as the test medium. The technique utilizes towing of inverted instrumented models in a hydrodynamic test basin. Data are presented on both the open cassegrain and the triply-folded horn-reflector antennas.

I. INTRODUCTION

The feasibility of operating a narrow beam tracking antenna without the environmental protection of a radome is dominated by the consideration of antenna tracking accuracy under the influence of wind-induced random disturbance torque. Although the wind power spectrum at a point may be quite variable and may depend somewhat upon the locality, for our purpose it is sufficient to assume a characteristic resembling a first order low-pass filter with a cut-off angular frequency ω_c in the range 0.12 to 3 radians per second.[1,2,3] That is, we assume the variable component of wind velocity to have a two-sided power-density spectrum of the form:

$$\Phi_{vv}(\omega) = \frac{1}{\pi} \frac{\omega_c V_1^2}{\omega_c^2 + \omega^2} \tag{1}$$

where V_1 is the standard deviation of the variational component of the wind velocity.

It is assumed that a satellite communications antenna must survive winds of 100 mph velocity. For compressible flow, Bernoulli's theorem can be expressed as

$$\frac{dp}{\rho} = -V\,dV,$$

where p is pressure, ρ is fluid density and V is the fluid free stream velocity. For an adiabatic process,

$$p = K\rho^{\gamma}$$

where K and γ are constants, γ being the ratio of specific heats. For dry air, $\gamma = 1.405$. Then, denoting the state values of a gas at stagnation by the subscript o,

$$\int_{p_o}^{p} \frac{dp}{\rho} = K\gamma \int_{\rho_o}^{\rho} \rho^{\gamma-2}\,d\rho = \frac{K\gamma}{\gamma - 1}\left[\rho^{\gamma-1} - \rho_o^{\gamma-1}\right]$$

or

$$\int_{p_o}^{p} \frac{dp}{\rho} = \frac{\gamma}{\gamma - 1}\left(\frac{p}{\rho} - \frac{p_o}{\rho_o}\right).$$

Bernoulli's theorem then gives

$$\frac{\gamma}{\gamma - 1}\frac{p}{\rho} + \frac{1}{2}V^2 = \frac{\gamma}{\gamma - 1}\frac{p_o}{\rho_o}.$$

Solving for V^2 and using the adiabatic gas law

$$V^2 = \frac{2\gamma}{\gamma - 1}\frac{p_o}{\rho_o}\left[1 - \left(\frac{p}{p_o}\right)^{(\gamma-1)/\gamma}\right].$$

Noting that the speed of sound C is given by $C^2 = \gamma p/\rho$,

$$V^2 = \frac{2C_o^2}{\gamma - 1}\left[1 - \left(\frac{p}{p_o}\right)^{(\gamma-1)/\gamma}\right].$$

Solving for the pressure ratio p/p_o and expanding in a Maclaurin series;

$$\frac{p}{p_o} = \left[1 - \frac{\gamma - 1}{2}\left(\frac{V}{C_o}\right)^2\right]^{\gamma/(\gamma-1)}$$

$$\frac{p}{p_o} = 1 - \frac{\gamma}{2}\left(\frac{V}{C_o}\right)^2 + \frac{\gamma}{8}\left(\frac{V}{C_o}\right)^4 - \frac{\gamma(2 - \gamma)}{48}\left(\frac{V}{C_o}\right)^6 + \cdots.$$

The ratio of the third term to the second term in the series is $V^2/4C_o^2$. For a free stream velocity of 100 mph = 147 ft/sec, C_o is approximately 1.018 C_f where the subscript f refers to free stream conditions. Under standard temperature and pressure then, $V_f^2/4C_o^2 = 0.0037$. For rounded bodies such as spheres and cylinders normal to the direction of flow the maximum pressure difference $|\ p - p_f\ | \approx 1.2\ (p_o - p_f)$ while

for bluff bodies $| p - p_f |$ may be locally as high as 1.7 $(p_o - p_f)$. Assuming the latter, $V^2/4C_o^2 = 0.010$; that is, for a free stream velocity of 100 mph at no point on the surface of the antenna does the third term in the series exceed one per cent of the second term. Since the series is convergent and alternating, the error in calculating dynamic pressure resulting from discarding all terms after the second must be less than 1 per cent. Then:

$$\frac{p}{p_o} = 1 - \frac{\gamma}{2}\left(\frac{V}{C_o}\right)^2 = 1 - \frac{1}{2}\frac{\rho_o}{p_o}V^2$$

or $p = p_o - \frac{1}{2}\rho_o V^2$. Thus the assumption of incompressibility leads to negligible error in calculating the forces and moments induced by winds up to 100 mph on a full scale antenna.

With a knowledge of the antenna structural and servo parameters, the pointing error resulting from a disturbing wind torque input can be predicted. In their generalized complex form, the angular displacement of the pointing vector, θ, can be related to the wind torque T by a system transfer function such that

$$K_{ij}(s) = \frac{T_i(s)}{\theta_j(s)} \tag{2}$$

where s is the Laplace transform variable and the indices refer to the antenna axes.

Little is known about the spatial distribution of instantaneous wind velocity, but if we can assume such variation to be negligible over the dimensions of an antenna; then, from Bernoulli's theorem for incompressible flow, we may write for the ith axis

$$T(t) = (\rho C_d A R/2)V^2(t) \tag{3}$$

where C_d is the drag coefficient, A is the antenna projected area, R is the length of the moment arm from the center of pressure to the antenna axis, all functions of the aspect angle φ, ρ is the density of air and V is the free stream wind velocity. Defining a wind torque coefficient for the ith axis

$$C_w = \rho C_d A R/2, \tag{4}$$

$T(t)$ may then be written

$$T(t) = C_w(\varphi)V^2(t). \tag{5}$$

$K_{ij}(s)$ is a complicated function of antenna and servo parameters, few of which have been evaluated for the antenna designs treated in

this paper. Consequently, we cannot calculate tracking error as a function of wind velocity for these antennas. However, because one of the most significant characteristics of an all-weather satellite communications antenna is its tracking performance in wind and because the values of C_w presented in this paper have little meaning unless related to antenna performance, it seems reasonable to make sufficient simplifying assumptions to reach an approximate functional relationship between C_w, V and tracking error such that on the basis of incomplete, preliminary design data, an estimate of wind performance can be made. We then assume:

(1.) Wind induced error about the vertical axis of the antenna is much greater than about the elevation or inclined axis. (This is a reasonable assumption because the wind torque and structural compliance are both much greater about the vertical axes.)

(2.) The structure is much more compliant about its rotational axes than about any other axis.

(3.) The foregoing is true and we need consider only the vertical axis and can neglect the coupling between axes; (2) can then be written

$$K_w(s) = [T(s)/\theta_a(s)] \tag{2'}$$

where $K_w(s)$ is the overall azimuth stiffness function

$\theta_a(s)$ is the azimuth pointing error.

Representing this simplified system as shown in the Appendix, the variance of the pointing error in the autotrack mode of operation is given by

$$\overline{\theta_a^2}(t) = \frac{8C_w^2V_o^2V_1^2}{\omega_c}\left[\frac{1}{2\pi j}\int_{-j\infty}^{j\infty}\frac{ds}{(1+s/\omega_c)K_w(s)(1-s/\omega_c)K_w(-s)}\right] \tag{6}$$

where V_o is the average wind velocity and V_1 is the standard deviation of the time variant component of wind velocity.

It is seen that the standard deviation of the antenna azimuth pointing error is proportional to the product $C_wV_oV_1$, but the integral cannot be evaluated because $K_w(s)$ involves unknown structural and servo parameters. Examination of the form of $K_w(s)$, however, reveals that the dominant term at low frequency is the azimuth structural stiffness K_a.

If $K(s)$ can be considered to be constant and equal to K_a over a frequency band extending well beyond the wind cut-off frequency, then the standard deviation of the antenna pointing error in the autotrack mode of operation is given by

$$\sigma(\varphi) = \frac{2V_oV_1C_w(\varphi)}{K_a} \tag{7}$$

This equation, though greatly oversimplified is nevertheless useful in preliminary antenna design and provides a basis for comparison of different configurations. Further discussion of this equation and an indication of its applicability appear in the Appendix.

The quantity C_w must be determined therefore, if the tracking performance in wind is to be estimated for a proposed antenna configuration. Similarly, the antenna overturning stability may be described in terms of an overturning moment coefficient $C_{wo}(\varphi)$ which may be defined for any convenient axes. The numerical values of C_w and C_{wo} for the most unfavorable orientation of an antenna may be used as a figure of merit for comparison of various antenna configurations.

II. MODEL TEST THEORY

Aerodynamic force and torque coefficients can be determined experimentally by measuring the forces and moments induced by fluid flow around a scale model. In such model tests it is important to maintain the same type of fluid flow as encountered in the full size antenna structure. The antenna configurations considered in this paper, particularly the triply-folded horn-reflector, have been designed to approximate a rounded body such as a sphere in so far as is practical. To the extent that this design effort was unsuccessful, the antenna is a bluff body; that is, for Reynolds Numbers N_{re} larger than about 1000, flow will separate at the largest cross section of the body and the drag coefficient C_d will be approximately constant at some fairly high value. However, to the degree that the faired contours of the antenna approximate a rounded body, a marked transition in the character of flow will be exhibited as the Reynolds Number is increased beyond some critical value, N_c. The critical Reynolds Number depends not only upon the shape of the body but also upon upstream turbulence. The greater the turbulence of the approaching fluid, the lower will be the value of N_c. For lack of better information we may assume for the present that N_c will be somewhere between 10^5 and 5×10^5, the approximate transition range for spheres and cylinders.

At fluid speeds in the approximate range of Reynolds Numbers from 10^3 to 10^5 the boundary layer on the upstream side of the body is laminar because of its extreme thinness and remains in contact with the surface of the body as far downstream as approximately the largest cross section of the body. Here the boundary layer fluid enters a region where the pressure increases in the direction of flow. The adverse pressure gradient forces the fluid away from the surface, i.e., the main stream separates from the body, creating a large wake area. As the

Reynolds Number is increased beyond N_c, the point of separation abruptly shifts farther back, reducing the wake area and thereby reducing the drag coefficient, C_d. The shift in separation point is due to the transition in the boundary layer from laminar to turbulent flow. The turbulent boundary layer, because of its increased momentum travels somewhat farther along the surface before the pressure causes it to separate again. There are then, two distinct regimes of flow, defined as

$$\text{subcritical} \quad -10^3 < N_{re} < 10^5$$

$$\text{supercritical} - N_{re} > 5 \times 10^5$$

where N_{re} is the Reynolds Number and the limits given above are estimates.

$$N_{re} = VD/\nu;$$

D is a characteristic linear dimension of the body and ν is the kinematic viscosity of the fluid.

Experiment has shown that the drag coefficient of a rounded or streamlined body in supercritical flow is relatively constant and is considerably lower than for subcritical flow. Air flow around a faired antenna structure of 2500 square foot aperture size is estimated to be supercritical at wind speeds higher than about 10 miles per hour. Since we are concerned with the effects of high wind velocity on antenna performance and survival, it is the values of C_w and C_{wo} determined for supercritical flow that are of interest.

Because the same type of flow encountered by the actual antenna must be reproduced in a scale model test and since the flow is in the supercritical region, i.e., $N_{re} > 5 \times 10^5$, the product of fluid speed and the model characteristic dimension must be >81 ft^2 per second if the test is to take place in air at 20°C. For a complex antenna shape, the dimension D, the smallest characteristic dimension of any area of the antenna whose drag force contributes significantly to the total induced forces or torques acting on the antenna is difficult to estimate accurately and may be much smaller than l the largest dimension of the antenna. Moreover, as indicated above, the critical Reynolds Number cannot be accurately estimated. Therefore, in selecting a model test facility, care must be taken to insure that the facility has the capability of providing flow velocity well in excess of the estimated requirement. The difficulty of testing in air may be shown by assuming a model size $l = 12$ inches and $l/D = 5$. The minimum required air velocity is then 275 mph or Mach .34 and the uncertainty in N_c and D makes the requirement for even higher speed a possibility. At these Mach

numbers, the third term in the power series expansion for the pressure ratio p/p_0 becomes significant with respect to the second term. That is, air at the Mach numbers likely to be encountered in wind tunnel testing must be considered a compressible medium and appropriate corrections must therefore be made to the test data before it can be applied to the full scale antennas.

If water is used as the test medium rather than air, the velocity requirement is reduced by a factor of 15 because of water's lower kinematic viscosity. The requirement for supercritical flow then becomes $VD > 5.4$ ft^2 per second. Because air at a free stream velocity of 100 mph can be considered to be incompressible (with negligible error as demonstrated above) the scaling from air to water presents no difficulties. The hydrodynamic test facilities of the Davidson Laboratory of Stevens Institute of Technology, Hoboken, New Jersey, provide the required flow conditions, and were used in making the measurements to be described.

III. MODELS AND INSTRUMENTATION

Of the three models of all-weather satellite communications antenna concepts that were constructed and tested, two are reported in this paper. These are shown in Figs. 1 through 3. Model "A" represents the triply-

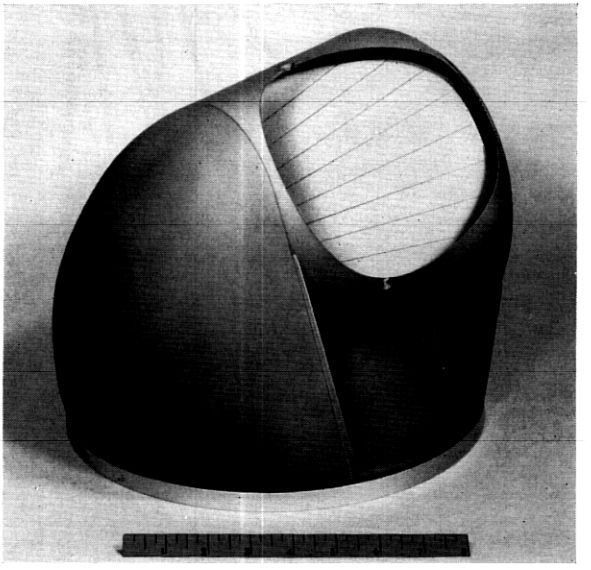

Fig. 1 — Model "A" with aperture cover removed.

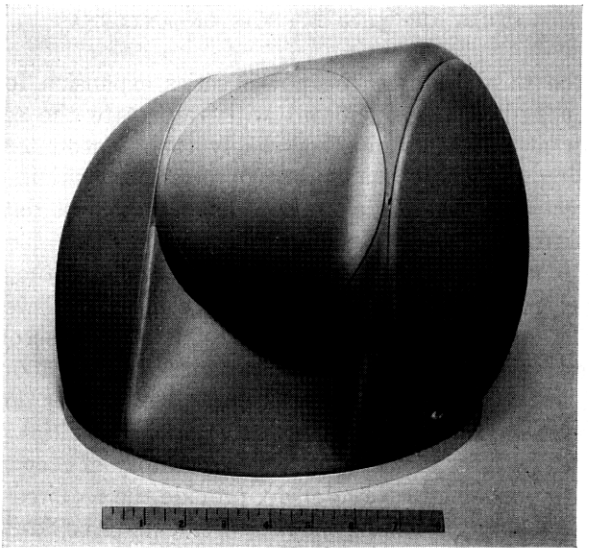

Fig. 2 — Model "A."

Fig. 3 — Model "B," the open cassegrain antenna.

folded horn-reflector antenna[5] and Model "B" is the open cassegrain antenna.[6] An aperture cover, of the same contour as the elevation drum, was installed on Model "A" in some of the test runs to determine the aerodynamic value of such a device.

Torque about the vertical axis, overturning moments about the antenna base and total drag were measured by means of a standard five component balance supplied by the testing facility. The inverted model mounted on the balance, was supported below the surface of the water. A large plate, simulating the ground plane at the surface of the water, was supported independently so that only the hydrodynamic forces acting on the model would be sensed by the balance. Fig. 4 shows a model mounted for testing.

The models also contained internal torque balances using constant stress cantilevers and linear differential transformers as seen in Figs. 5, 6, and 7. Fig. 8 defines the orientation of antenna axes with respect to flow direction.

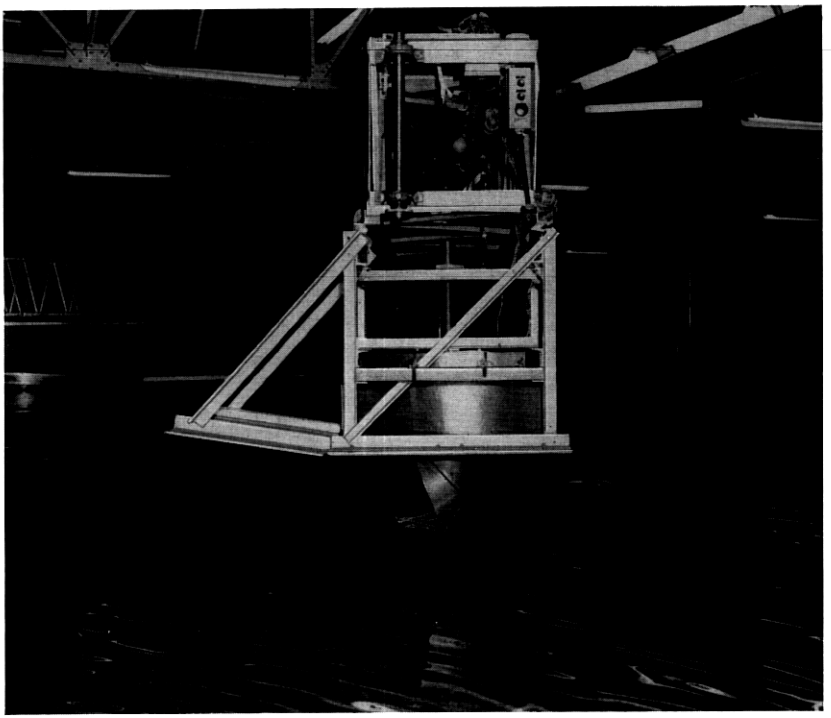

Fig. 4 — Model "B" about to be lowered into the tank for test run.

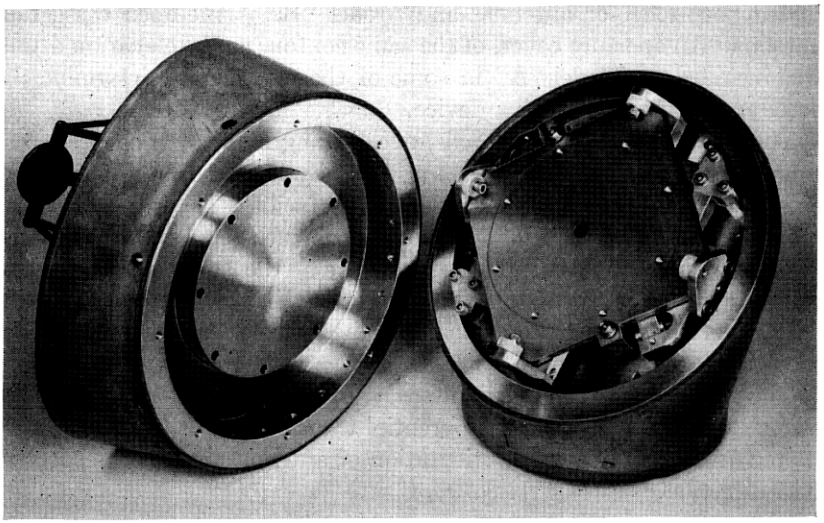

Fig. 5 — Model "B," showing internal uncoupled three component balance.

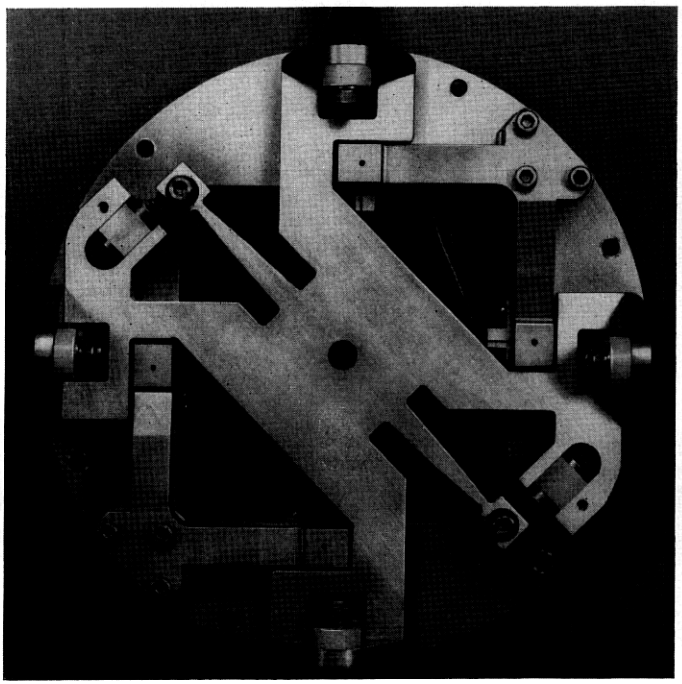

Fig. 6 — Uncoupled three component balance for Model "B."

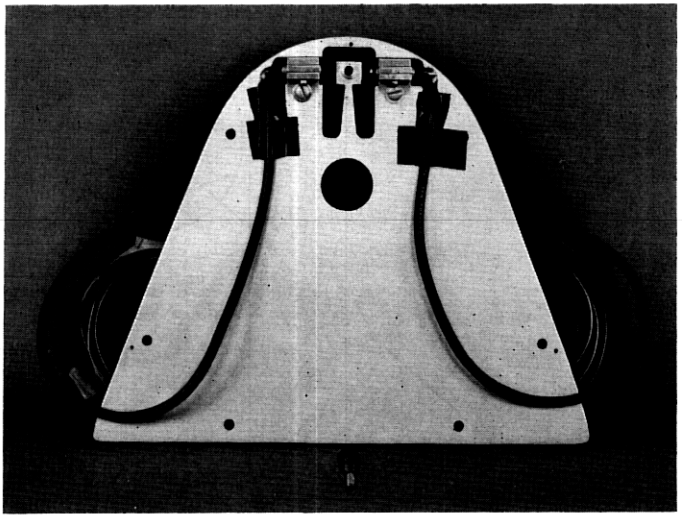

Fig. 7 — Elevation balance plate assembly for Model "A."

IV. TEST PROCEDURE

The required flow velocity was established by towing the model through the test tank at various constant velocities to obtain values for the drag coefficient, C_d . From a plot of C_d versus V, the transition speed was determined. The criterion used for establishing the appropriate test velocity for each model was a constant drag coefficient with increasing Reynolds Numbers.

Data runs were then made at the appropriate velocity for various orientations of the model. The outputs of the external and internal torque balances were recorded for each run. Fig. 9 shows a data run in progress.

V. TEST RESULTS

The experimental results for the two antenna concepts are presented in Fig. 10 through 19 as plots of wind torque coefficients versus wind azimuth aspect angle for various orientations of the elevation or inclined (slant) axis. The most significant quantity for both antennas is the wind torque coefficient about the vertical axis. Wind induced torque about the elevation (or inclined) axis of the two models is relatively small.

Precise values of weight and center of mass are not available during the preliminary design of an antenna, but on the basis of preliminary

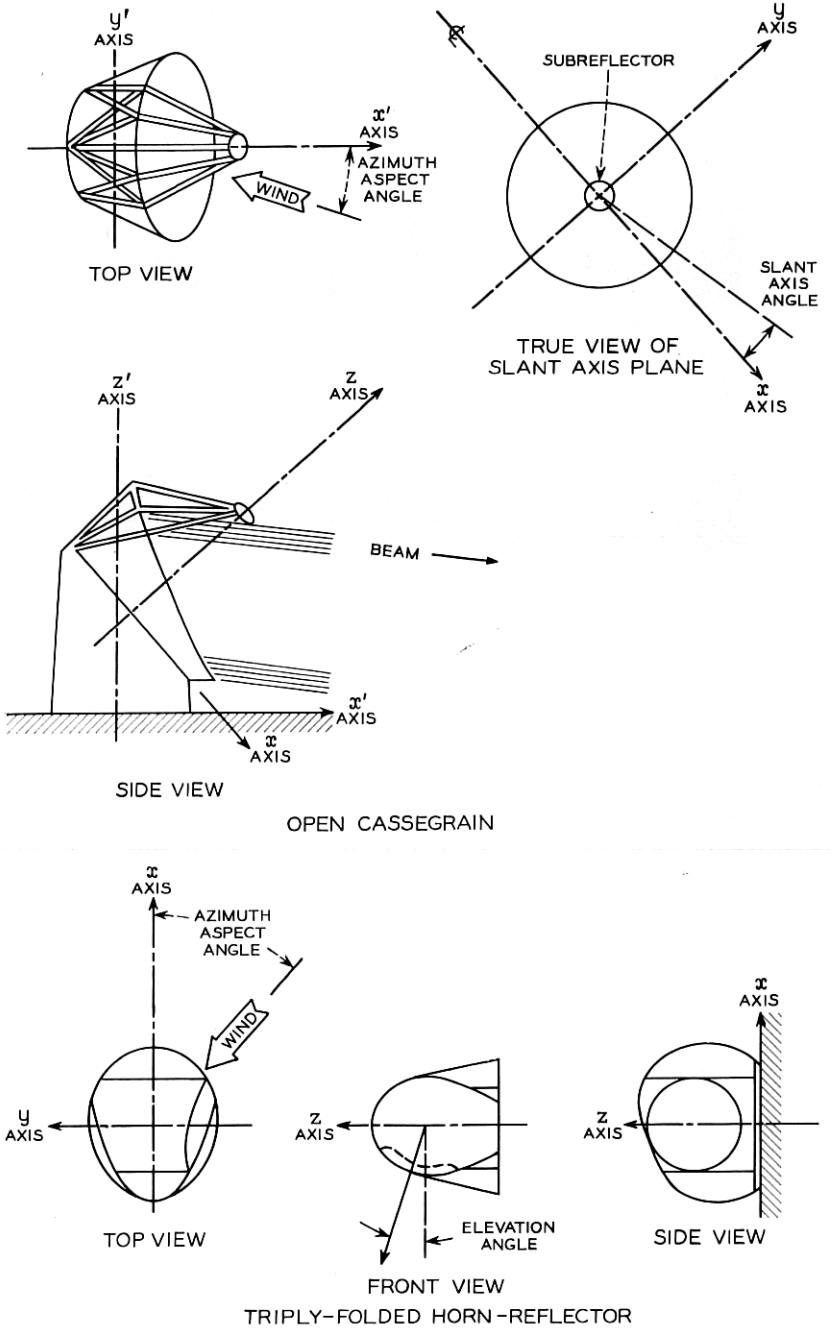

Fig. 8 — Axis orientation.

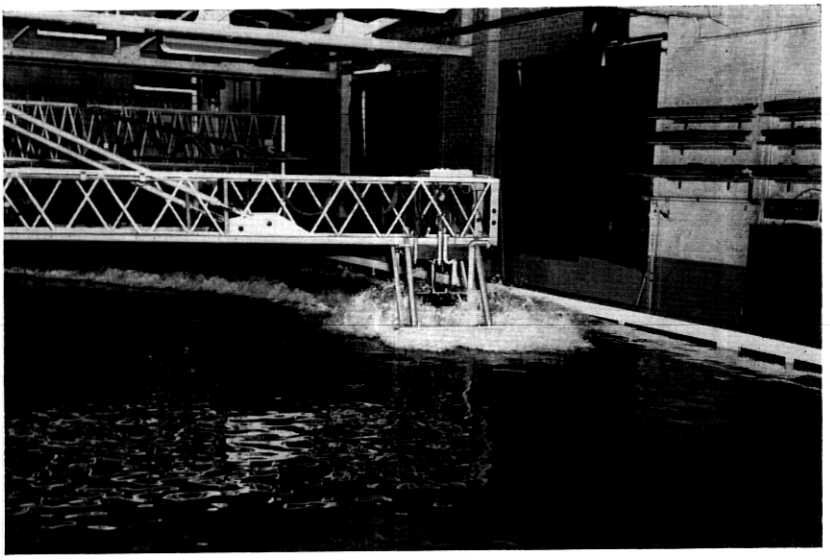

Fig. 9 — Data run.

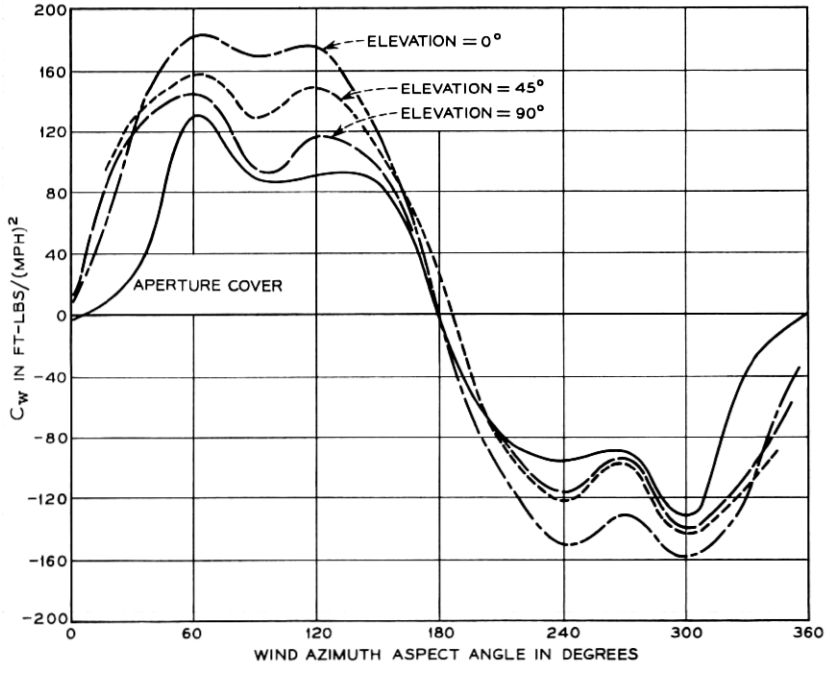

Fig. 10 — Azimuth torque — Model "A."

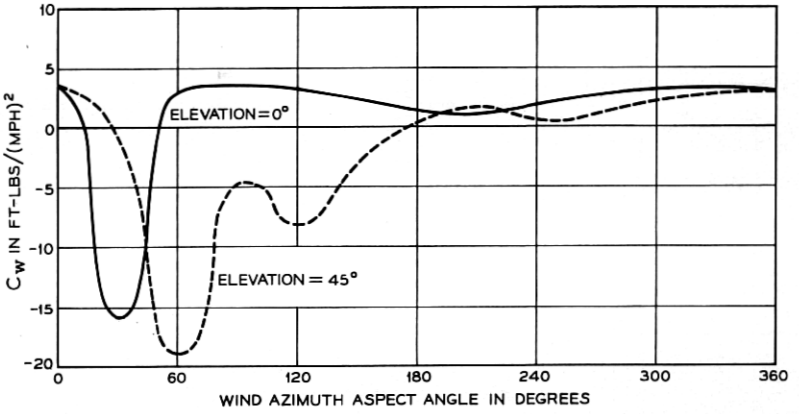

Fig. 11 — Elevation torque — Model "A."

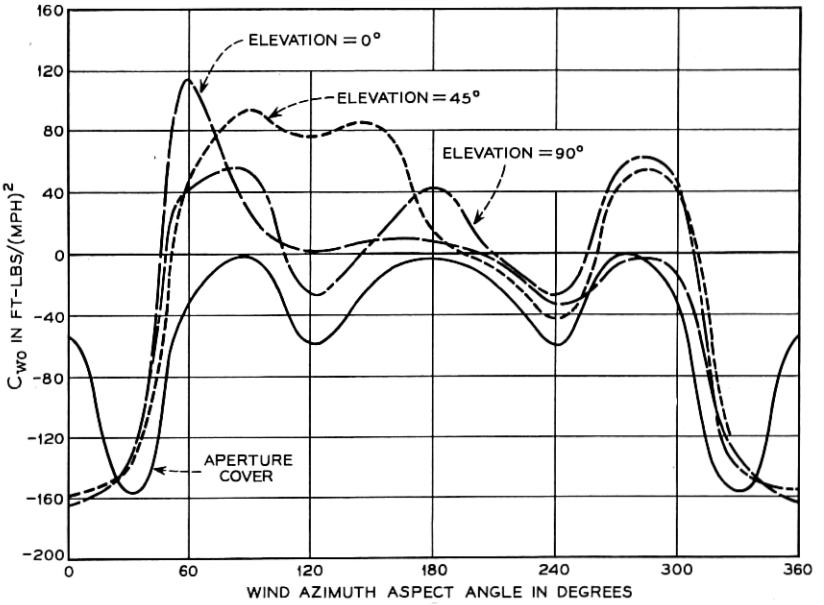

Fig. 12 — Overturning moment about transverse axis (Y) — Model "A."

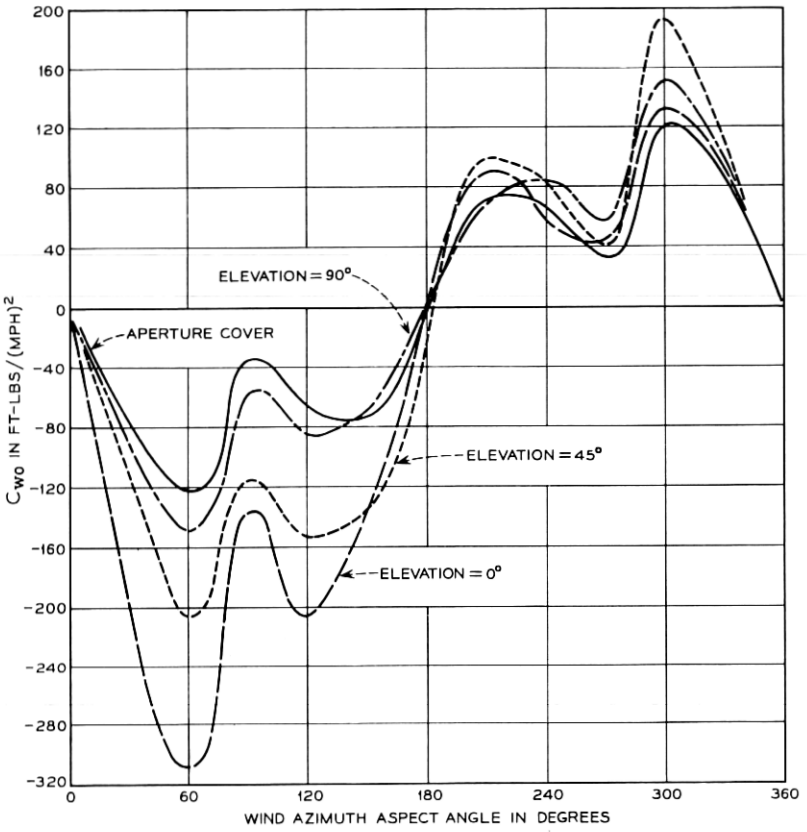

Fig. 13 — Overturning moment about longitudinal axis (X) — Model "A."

estimates, the maximum wind overturning moments and the resisting stability moments can be fairly accurately predicted. These have been calculated for the two models here considered and are listed in Table I for wind velocity of 100 mph.

To make the plotted test data meaningful in terms of antenna performance, some comparative values may be computed by assuming that the pointing error about the vertical axis is given by (7), that the standard deviation, V_1, of the wind velocity is 50 per cent of the average value, V_o, and by choosing a representative value of the stiffness, K_a. For the Andover Telstar antenna, $K_a = 2 \times 10^9$ ft-lbs per radian. It is conservative then to assume the same value for the relatively more compact and rigid structures considered in this paper, provided that a

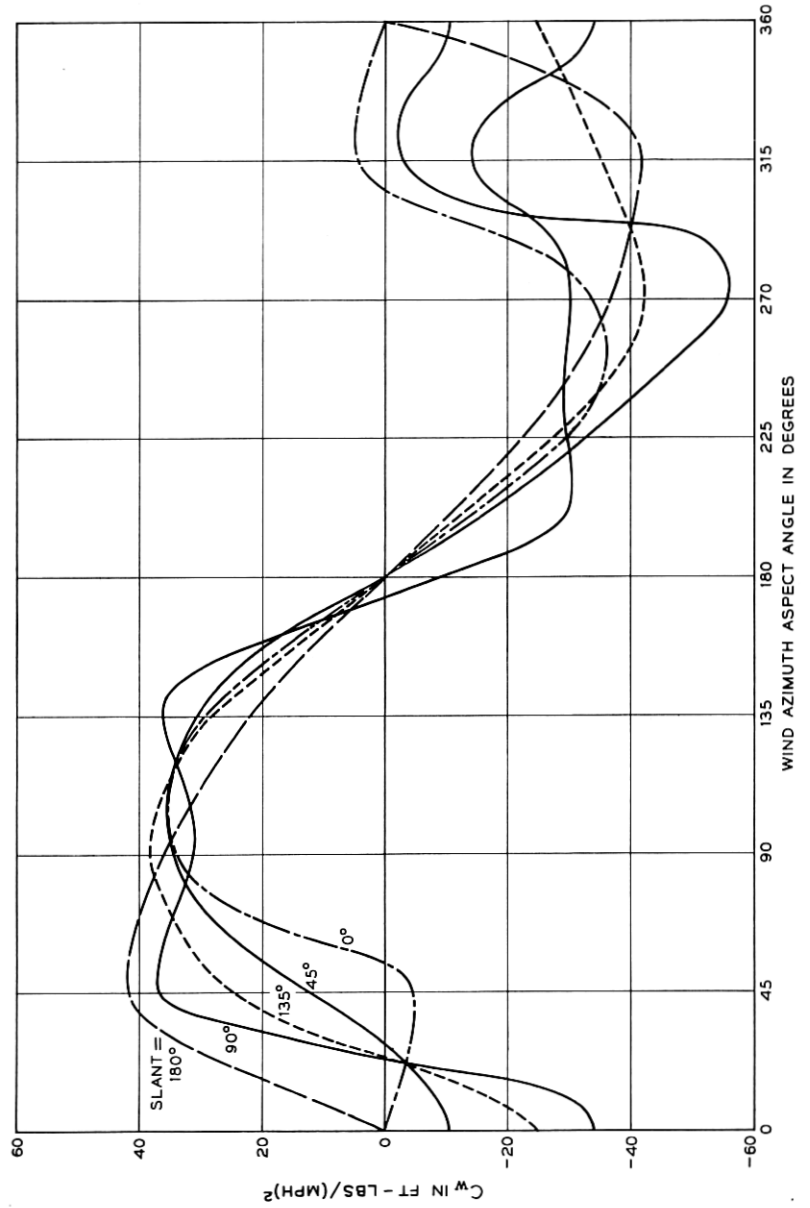

Fig. 14 — Open cassegrain — wind torque about vertical axis.

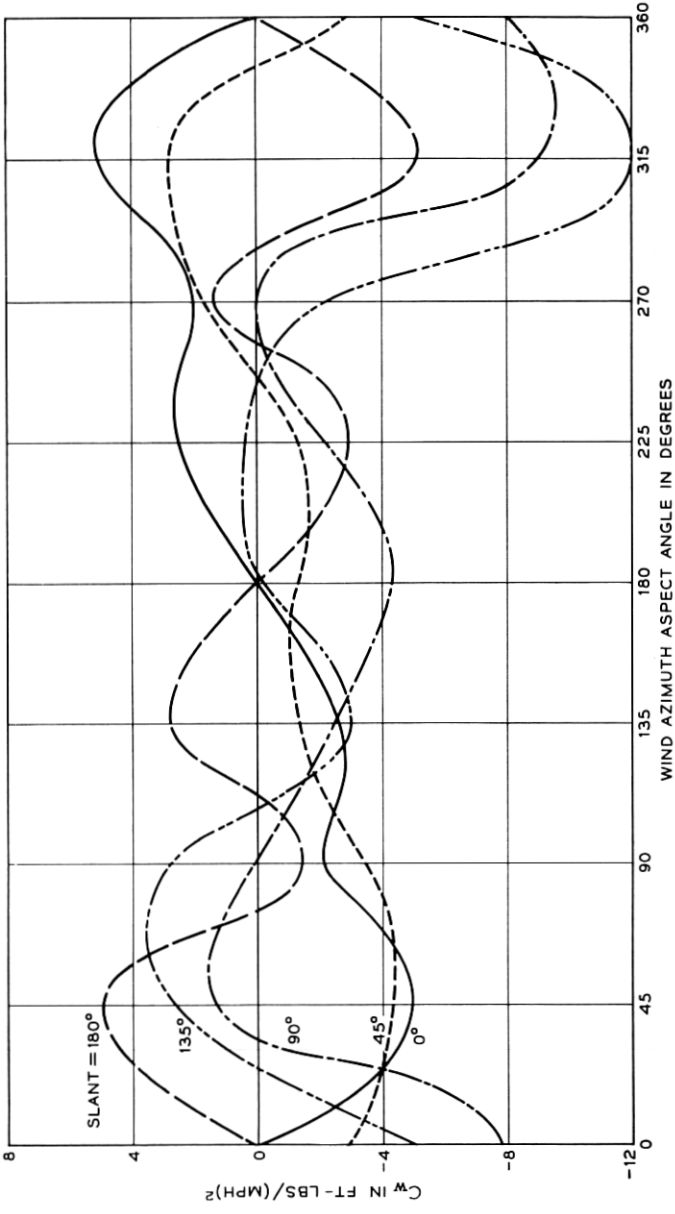

Fig. 15 — Open cassegrain — wind torque about slant axis.

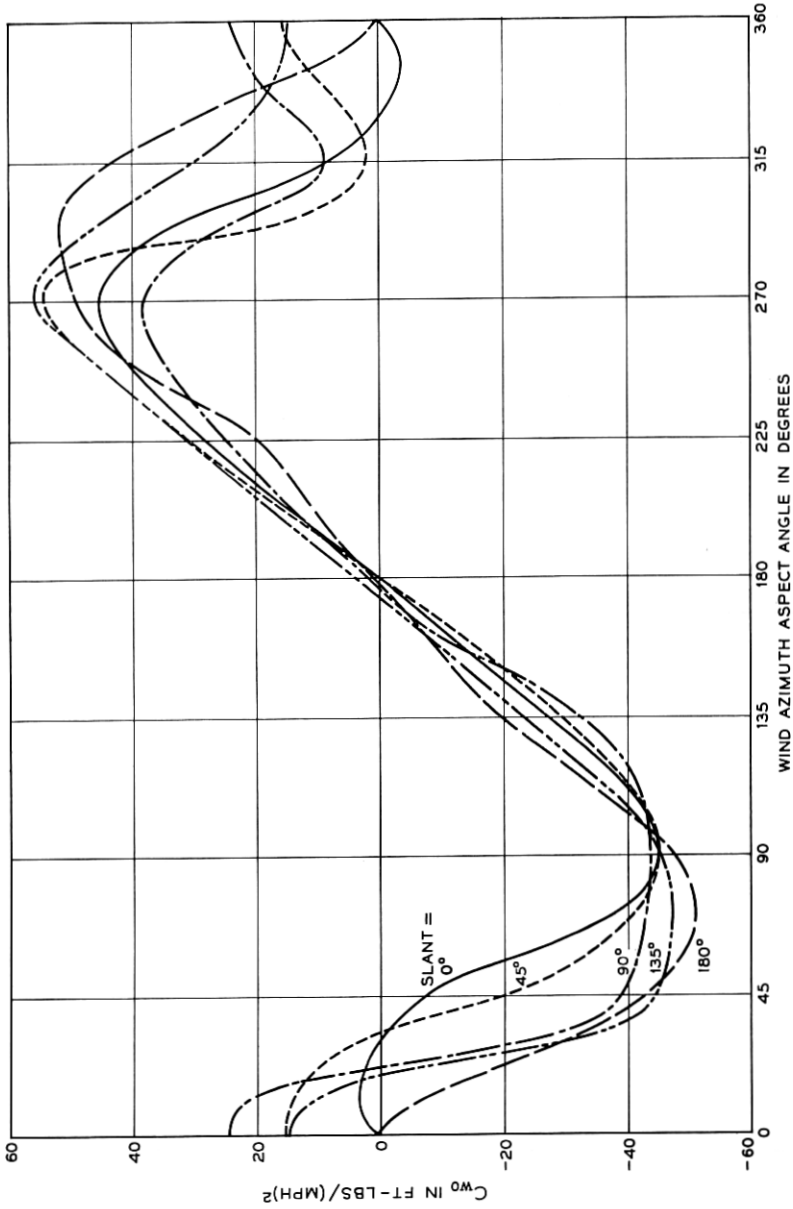

Fig. 16 — Open cassegrain — reaction moment on slant rail about x-axis due to wind on reflector section.

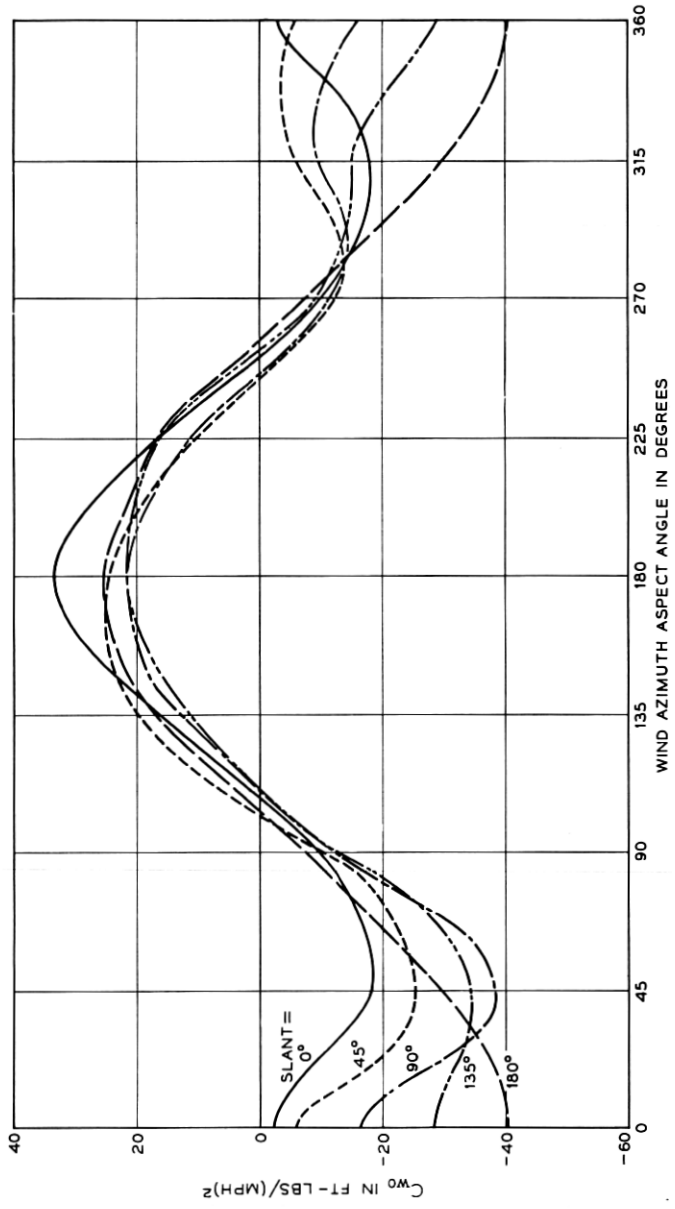

Fig. 17 — Open cassegrain — reaction moment on slant rail about y-axis due to wind on reflector section.

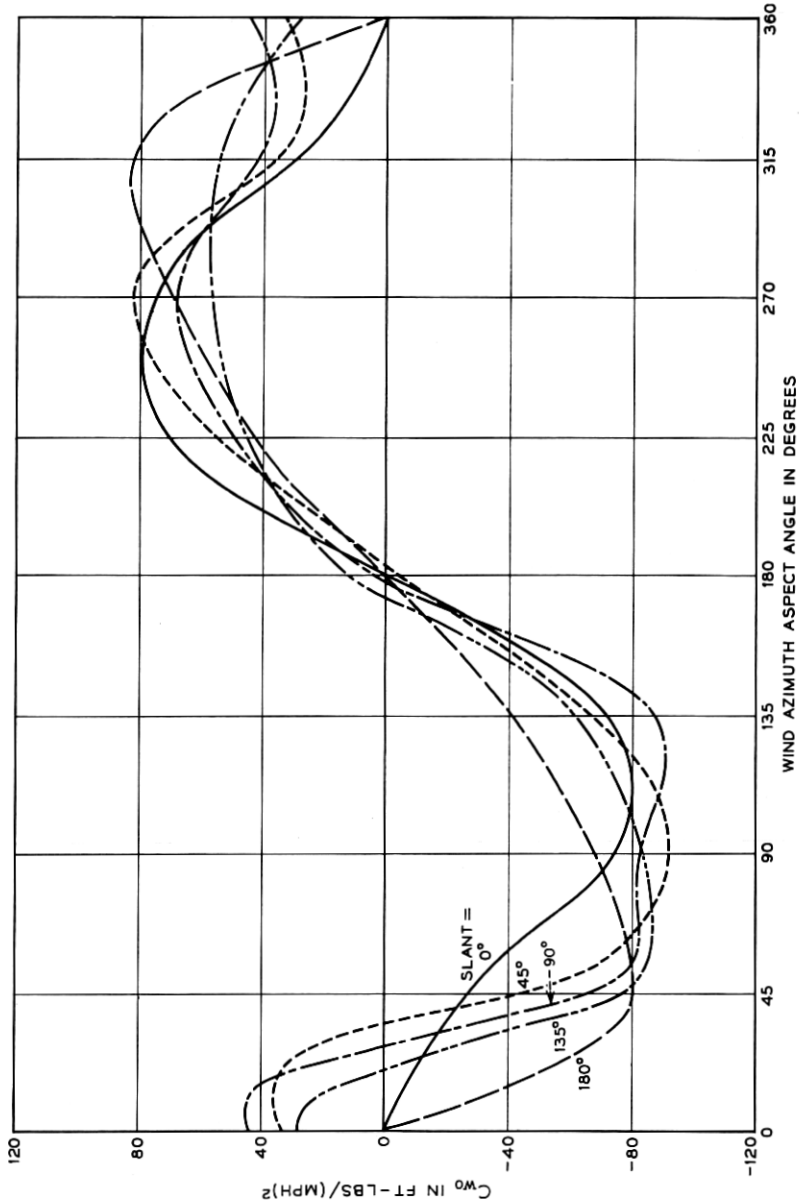

Fig. 18 — Open cassegrain — wind overturning moment about x'-axis in base.

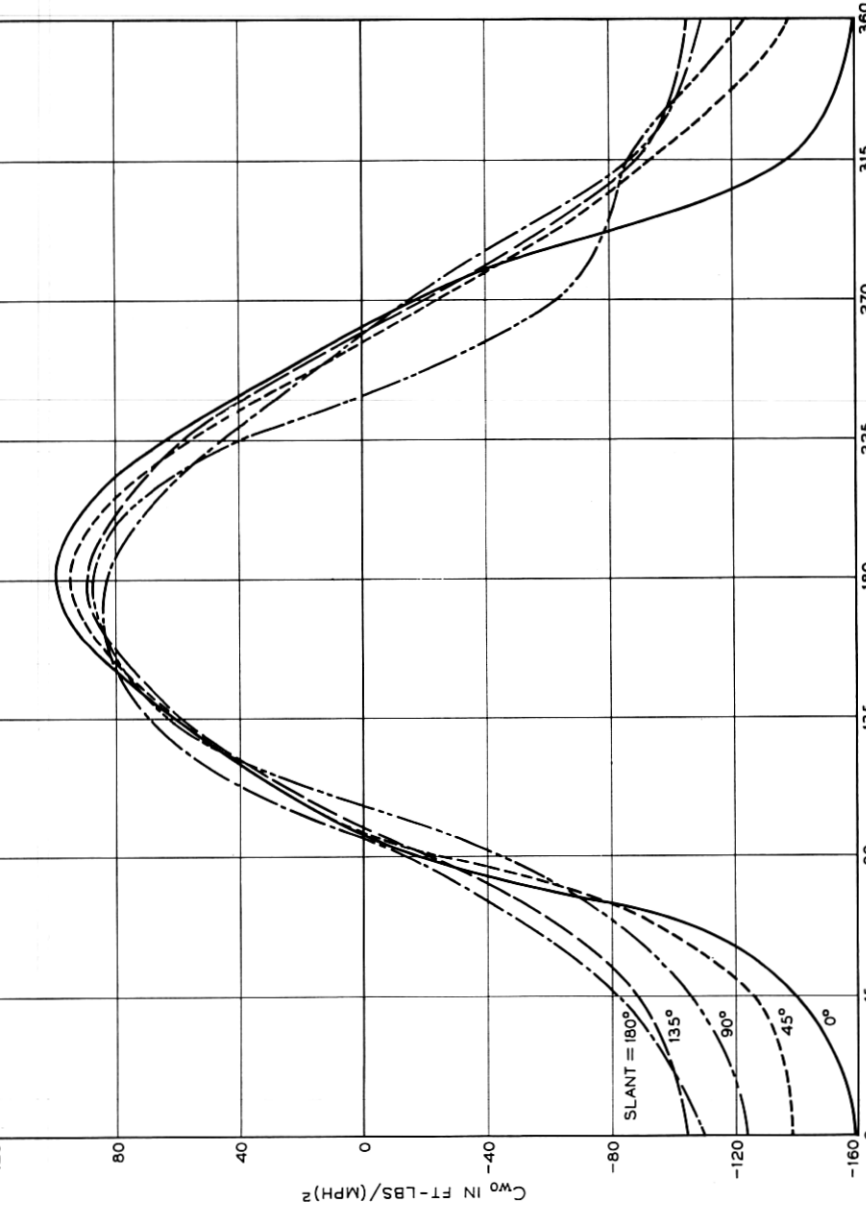

Fig. 19 — Open cassegrain — wind overturning moment about y'-axis in base.

TABLE I

WIND EFFECTS ON ALL-WEATHER SATELLITE COMMUNICATIONS ANTENNAS

		Overturning Moment at 100 mph ft-lbs	Stability Moment ft-lbs	Overturning Safety Factor	C_w for Vertical Axis ft-lbs/(mph)^2	Wind* Speed to Stall Antenna Drives, mph	Wind Speed‡ for 0.01° Pointing Error mph
Triply-folded horn-reflector antenna (2250 ft^2 aperture)**	With aperture cover or in "stow" position	1.56×10^6	24×10^6	15	132	95	$V_o = 51$ $V_1 = 25.5$
	Without aperture cover	3.1×10^6	19×10^6	6	184	80	$V_o = 43$ $V_1 = 21.5$
Open cassegrain antenna (2460 ft^2 aperture)**	Entire antenna	1.6×10^6	5.6×10^6	3.5	57.5	71	$V_o = 47$† $V_1 = 23.5$
	Reflector section only	$.685 \times 10^6$	1.7×10^6	2.5			

* Two 25-hp drives assumed. Available drive torque for triply-folded antenna is 1.2×10^6 ft.-lbs. Open cassegrain design assumes higher angular velocity, limiting available drive torque to about 2.9×10^5 ft.-lbs.

** The aperture sizes presented were arbitrarily selected and no electrical equivalence is indicated.

† See Appendix, p. 1365.

‡ V_o is the average wind speed; V_1 is the standard deviation of the variable component of wind speed.

correction is made to account for the open cassegrain subreflector support (see Appendix).

The wind velocity at which the standard deviation in antenna pointing error for the vertical axis equals 0.01° is given in Table I for the two antennas tested. The stall torque wind speed is also presented for each antenna. This is the wind speed at which wind induced torque about the vertical axis equals available drive torque and is based on the assumption that two 25-hp motors provide the azimuth drive. It will be noticed that the stall torque wind speed for the open cassegrain antenna is lower than might be expected from a comparison of wind torque coefficients. This results from the assumption of a lower drive gear ratio which would permit relatively higher antenna angular velocity and possible elimination of the zenith "tracking dead-zone" which is characteristic of all antennas with a vertical axis.

VI. CONCLUSIONS AND SUMMARY

The test results indicate that the wind torques induced about the rotational axes of the antennas are not excessive, and that with sufficient structural rigidity, tracking performance will be adequate. As pointed out above, however, the variation in instantaneous wind velocity over the dimensions of the antenna has been neglected. If an appreciable variation were found to exist the wind torque input to an antenna might be altered significantly, depending upon the correlation between the time and spatial variation in wind velocity.

Both antenna configurations are inherently stable in wind up to 100 mph.

VII. ACKNOWLEDGMENTS

The author wishes to thank Dr. P. Ward Brown of the Davidson Laboratory for his assistance in organizing the test program. The work of Dr. F. A. Russell and Dr. W. H. W. Ball on wind loading for the Andover antenna was an inspiration and aid in the hydrodynamic study. The success of this program was due in large measure to Messrs. J. H. Cave and H. W. Boschen whose assistance in the design and construction of the test models proved invaluable.

APPENDIX

Wind-Induced Pointing Error in the Autotrack Mode

The azimuth pointing error is given by

$$\theta_a(s) = [T(s)/K_w(s)]$$

where $T(s)$ is the wind torque disturbance, and

$K_w(s)$ is the overall azimuth system transfer function.

Representing the system in autotrack mode by a mechanical schematic (Fig. 20(a)) and an electrical analog (Fig. 20(b)) the transfer function can be written

$$K_w(s) = \left[R_1 + \frac{K_a K_g A F_s - K_a^2 R_3}{R_2 R_3 - K_g^2} \right] \tag{8}$$

where $R_1 = s^2 J_a + sB_a + K_a$

$R_2 = s^2 J_c + sB_c + K_a + K_g$

$R_3 = s^2 J_m + sB_m + K_g$

A is the servo torque gain

$F_s(s)$ is the servo shaping function

K, J and B are the stiffness, inertia and resistance respectively, and

the subscripts refer to the motion of the horn or reflector section (a), the motion of the cradle or pedestal (c), the motion of the gear boxes (g), and the motion of the drive motors (m).

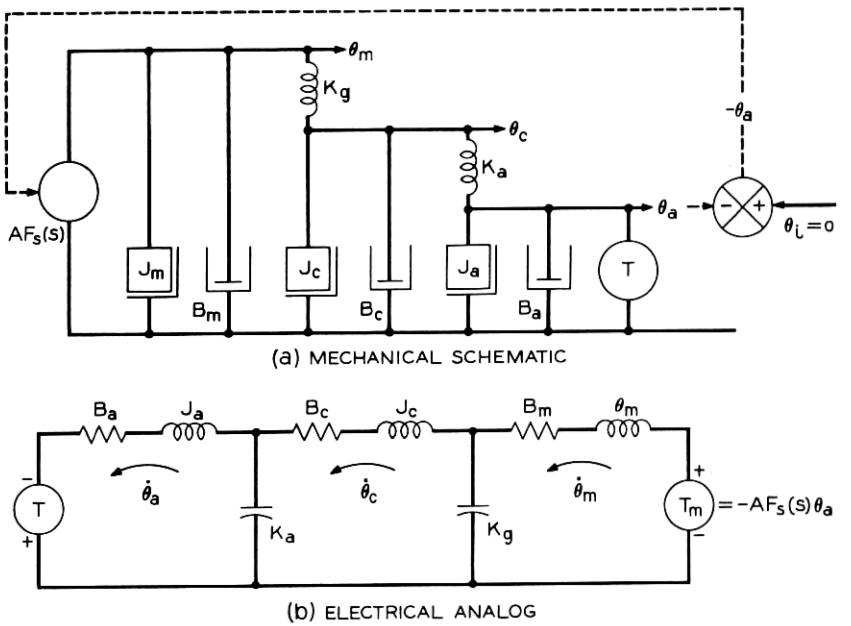

Fig. 20 — (a) Mechanical schematic, (b) electrical analog.

The time-variant input torque $T(t)$ is given by

$$T(t) = C_w V^2(t) = C_w[V_o^2 + 2V_o V_1(t) + V_1^2(t)]. \quad (9)$$

Noting that the constant term $C_w V_o^2$ produces no error in the auto-track mode, and assuming that $V_1^2(t) \ll 2V_o V_1(t)$, the transfer function from gust velocity to torque is $2C_w V_o$. The wind gust spectral power density is assumed to be of the form

$$\Phi_{vv}(s) = \frac{V_1^2 \omega_c}{\pi(\omega_c^2 - s^2)}. \quad (10)$$

For linear systems, the power density function of the output is equal to the power density function of the input multiplied by the square of the transfer function. The wind torque spectral density is therefore,

$$\Phi_{TT}(s) = 4C_w^2 V_o^2 \Phi_{vv}(s) \quad (11)$$

and the pointing error spectral density is

$$\Phi_{aa}(s) = \frac{4C_w^2 V_o^2 \Phi_{vv}(s)}{|K_w(s)|^2}. \quad (12)$$

The pointing error variance is then

$$\overline{\theta^2}_a(t) = 2\pi \frac{1}{2\pi j} \int_{-j\infty}^{j\infty} \frac{\Phi_{TT}(s)}{|K_w(s)|^2} ds. \quad (13)$$

Substituting for $\Phi_{TT}(s)$,

$$\begin{aligned} \overline{\theta^2}_a(t) &= \frac{4C_w^2 V_0^2 V_1^2}{\pi\omega_c} 2\pi \left[\frac{1}{2\pi j} \int_{-j\infty}^{j\infty} \frac{ds}{(1 - s^2/\omega_c^2)|K_w(s)|^2}\right] \\ &= \frac{8C_w^2 V_o^2 V_1^2}{\omega_c} \left[\frac{1}{2\pi j} \int_{-j\infty}^{j\infty} \frac{ds}{(1 - s^2/\omega_c^2)|K_w(s)|^2}\right]. \end{aligned} \quad (14)$$

Since, for $s = j\omega$,

$$|K_w(s)|^2 = K_w(j\omega)K_w^*(j\omega) = K_w(j\omega)K_w(-j\omega)$$

$$|K_w(s)|^2 = [K_w(s)K_w(-s)],$$

we may write finally:

$$\overline{\theta^2}_a(t) = \frac{8C_w^2 V_o^2 V_1^2}{\omega_c} \left[\frac{1}{2\pi j} \int_{-j\infty}^{j\infty} \frac{ds}{(1 + s/\omega_c)K_w(s)(1 - s/\omega_c)K_w(-s)}\right]. \quad (15)$$

The standard deviation of the error is given by the square root of the variance.

The integral

$$\frac{1}{2\pi j}\int_{-j\infty}^{j\infty}\frac{ds}{(1+s/\omega_2)K_w(s)(1-s/\omega_c)K_w(-s)}$$

can be evaluated analytically on the basis of the residue theory, as well as either graphically, or numerically.[4] A computer program has been written and used for evaluating this integral with TSX-1 antenna servo parameters. The results obtained are peculiar to that antenna and are therefore not applicable to the antennas under discussion here. Having no precise values for the terms contained in $K_w(s)$, we can nevertheless obtain an estimate of the performance of an antenna in wind by assuming the overall antenna transfer function to be constant over the frequency band extending to perhaps a decade beyond ω_c.

Considering the transfer function, (8), and the schematics, one can see that the term R_1 is the contribution of the antenna compliance and the inertia of the reflector section. If $\dot{\theta}_c = 0$, $K_w(s) = R_1(s)$, and at low frequency, $R_1(s) \approx K_a$.

The magnitude of the other term in $K_w(s)$ depends upon the torque gain, A, and shaping function $F_s(s)$. With error integration in the shaping, AF_s is large for small ω and it is reasonable to assume that the real part of the term

$$\frac{K_aK_gAF_s - K_a^2R_3}{R_2R_3 - K_g^2}$$

is positive and the imaginary part is small compared with K_a over the desired frequency band. With these assumptions we conclude that K_w is positive-real and that $|K_w| \geqq K_a$ in the frequency range of interest for the calculation of wind induced pointing error.

For $K_w(s)$ then, we substitute K_a in (15), yielding

$$\overline{\theta^2}_a(t) = \frac{8C_w^2V_o^2V_1^2}{K_a^2\omega_c}\left[\frac{1}{2\pi j}\int_{-j\infty}^{j\infty}\frac{ds}{1-s^2/\omega_c^2}\right]$$

$$= \frac{4C_w^2V_o^2V_1^2}{K_a^2},$$

so that

$$\sigma_a = \frac{2C_wV_oV_1}{K_a}.$$

In the case of the TSX-1 antenna, this approximation coincides with the results obtained through computer evaluation of the integral (using

measured antenna parameters) for $\omega_c = 0.6$ rad per second and holds to ± 50 per cent for $0.125 \leqq \omega_c \leqq 1.85$. The correspondence can be expected to be at least as good for the relatively stiffer and lighter all-weather antennas discussed in this paper.

In the case of the open cassegrain antenna however we must take into account the compliance of the subreflector support structure when computing the wind induced pointing error. Flow around the tubular support members is in the transition region between 10 and 50 mph wind speed, so we conservatively assume the flow to be always subcritical. Structural analysis has shown that under these conditions, C_W/K due to subreflector motion is 50×10^{-9} radians per $(\text{mph})^2$ referred to the antenna pointing vector. Assuming for the rest of the structure $K_a = 2 \times 10^9$ ft-lbs per radian and $C_W = 56$ ft-lbs per $(\text{mph})^2$, the adjusted C_W/K_a is 78×10^{-9} radians per $(\text{mph})^2$.

REFERENCES

1. Titus, J. W., Wind Induced Torques Measured on a Large Antenna, NRL Report 5549, Dec., 1960.
2. Lumley, J. L., and Panofsky, H. A., The Structure of Atmospheric Turbulence, Interscience Monograph, 1964.
3. Barton, D. K., RCA Final Report, Instrumentation Radar AN/FPS-16(XN-1), Evaluation and Analysis of Radar Performance, ASTIA Report No. 212125, March 19, 1959.
4. Newton, G. C., Gould, L. A., and Kaiser, J. F., *Analytic Design of Linear Feedback Controls*, Wiley, 1957.
5. Giger, A. J., and Turrin, R. H., The Triply-Folded Horn Reflector: A Compact Ground Station Antenna Design for Satellite Communications, B.S.T.J., this issue, pp. 1229–1253.
6. Denkmann, W. J., Geyling, F. T., Pope, D. L., and Schwarz, A. O., The Open Cassegrain Antenna: Part II. Structural and Mechanical Evaluation, B.S.T.J., this issue, pp. 1301–1319.